Int. J. Electrochem. Sci., 14 **(2019)** 10622 – 10632, doi: 10.20964/2019.11.22

International Journal of
ELECTROCHEMICAL
SCIENCE
www.electrochemsci.org

Modification of Lithium Iron Phosphate by Carbon Coating

Zheng Zhang, Mingming Wang, Junfeng Xu, Fangchang Shi, Meng Li and Yanmin Gao[*]

School of Materials Science and Engineering, Jiangsu University of Science and Technology, Jiangsu, Zhenjiang 212003, China
[*]E-mail: 1571539864@qq.com

Received: 9 June 2019 / *Accepted:* 15 August 2019 / *Published:* 7 October 2019

Lithium Iron Phosphate ($LiFePO_4$) for lithium-ion batteries is considered as perfect cathode material for various military applications.Carbon coating has a great influence on the properties of lithium iron phosphate. In this paper, the effects of in-situ carbon coating and non-in-situ carbon coating on the structure and properties of lithium iron phosphate were analyzed.For $LiFePO_4$/C synthesized by carbon coating, no matter it is non-in-situ coating or in-situ coating, it can improve the electrochemical performance of $LiFePO_4$. In this paper, ascorbic acid was used as the carbon source, and the sample coating layers formed by in-situ carbon coating and non-in-situ carbon coating were 10nm and 20nm respectively. Through the electrochemical measurements, In situ carbon coated and non-in-situ carbon coated lithium iron phosphate, the specific capacity of charge and discharge for the first time reached 125 $mAh \cdot g^{-1}$ and 112 $mAh \cdot g^{-1}$ respectively at the rate of 0.1C..Meanwhile, comparing the two coating methods, The structure and properties of in-situ carbon coating are better than those of non-in-situ carbon coating.

Keywords: lithium iron phosphate, In situ carbon coating, Non-in-situ carbon coating, electrochemical performance

1. INTRODUCTION

The rapid development of today's society has made people's demand for renewable energy more and more intense, and some traditional non-renewable resources are no longer sufficient for the development of society. The $LiFePO_4$ cathode material with olivine structure will be the most promising lithium ion battery [1]. The biggest advantage of lithium iron phosphate battery [2] is that it has higher specific energy density, longer charging and discharging platform [3], etc. The most important thing is to overcome the shortcomings of poor safety and pollution of lithium batteries, and it is a promising secondary battery [4]. However, the low electron conductivity (298K, $10^{-9}s \cdot cm^{-1}$), low lithium ion transport rate (10^{-14}~10^{-16} $cm^2 \cdot s^{-1}$) and low vibrational density limit the performance of lithium iron phosphate cathode materials. Therefore, it is necessary to modify the cathode material of lithium iron

phosphate [5-6]. At present, three most commonly used modification methods are ion doping [7-9], nano-modification or special morphology modification and carbon coating [10-12] on the surface of the material.

Carbon coating is a particularly common way to improve the electrochemical performance of $LiFePO_4$. The benefits of carbon coating are Carbon coating can not only improve the conductivity of the sample, but also inhibit the growth of crystal grains at high temperature and reduce the agglomeration effect, thereby refining the crystal grains, achieving the dual effects of improving its structural characteristics and improving its electrochemical performance. The carbon coating method is very convenient and feasible. Generally, the pure $LiFePO_4$ has a lower specific capacity due to the limitation of its structure. The addition method (in situ coating and non-in situ coating) of carbon material also has a great influence on its properties, which leads to the thickness of carbon layer coated with it, so this paper mainly discusses the influence of carbon coating form on the structure and properties of $LiFePO_4$/C [13].

Non-in-situ coating refers to the synthesis of $LiFePO_4$ from lithium source, phosphorus source and iron source by hydrothermal method, supplemented by ball milling to synthesize $LiFePO_4$/C, at high temperature so that the carbon source is attached to the surface of the sample, and the conductivity of the carbon source is improved by sintering. The advantage of the non-in situ carbon coating is that the carbon source is directly added to the $LiFePO_4$ powder, and the operation is simple and convenient. In situ carbon coating refers to the addition of carbon source to the preparation of $LiFePO_4$ precursor. The advantage of in-situ carbon coating is that the carbonation of carbon source can be used to inhibit the growth of crystal, alleviate the agglomeration of particles and improve the electronic conductivity between particles in the process of hydrothermal preparation. In-situ carbon coating is also a relatively effective carbon coating form. The advantage is that the template effect of the carbon source can be used to guide the growth and optimization of the sample morphology.

2. EXPERIMENTAL

2.1 experimental method

Using non-in situ coating method [14], the ratio of n($LiOH:FeSO_4:H_3PO_4$) = 3:1:1 (not adding carbon source in the synthesis process) was synthesized by hydrothermal method. The obtained turbid solution was washed and precipitated many times with ethanol and deionized water, and the powder sample was obtained by vacuum drying, and then ascorbic acid was used as carbon source [15]. While maintaining the other experimental conditions unchanged, weigh 5% ascorbic acid of $LiFePO_4$ powder mass, mix ball milling with a star ball mill for 3h, rotate at 300 r/min, and dry the mixed powder sample in a tube. Nitrogen (protective gas) was pre-sintered at 300℃ for 3h, and then sintered at 650℃ for 6h to carbonize ascorbic acid, adhere to the surface of $LiFePO_4$, and improve the conductivity of the sample.In situ carbon coating refers to the addition of carbon sources in the synthesis of LiFePO4 precursors, and the remaining steps are consistent with the above methods.

2.2. Structure characterization and electrochemical evaluation

The surface morphology and element distribution of the ZEISS Merlin Compact were observed by scanning electron microscopy-energy spectroscopy (SEM-EDS). The metallographic structure was observed by transmission electron microscopy (TEM) using JEM-2100F (JEM, Japan). X-ray diffraction (XRD) spectra were recorded with a D8 advanced diffractometer (Bruker, Germany). The scanning speed is 3°/min, and the scanning range from 15°~60°. Raman spectroscopy was recorded with an InVia Raman microscope (Renishaw, UK).Micro-FTIR was recorded with an NICOLET iN10 (agilent, USA).

2.3 Electrochemical characterization test

The cycle performance of the battery was tested by battery test system (LANDCT2001A). The current density was 1C , voltage range was 2.4 ~ 4.4V and the turn-off current was 0.02C. At the same time, the rate performance of the battery was also tested. the current density was controlled at 0.1~5C and the voltage was controlled at 2.4 ~ 4.4V during the test. Cyclic volt-ampere curve and electrochemical impedance measurement were recorded on electrochemical workstation (VSP-300). The scanning rate of cyclic volt-ampere curve was 0.1mV/s, and the range of electrochemical impedance measurement (EIS) was 0.01 ~ 100KHz.

2.4 Battery assembly

First, the prepared $LiFePO_4$ cathode composites, polyvinylidene fluoride and carbon black (Super P) were uniformly mixed in NMP solution according to the mass ratio of 8:1:1, and the uniform slurry was obtained. Secondly, the paste was coated on aluminum foil and dried in 80 °C oven to obtain cathode sheet. Third, the cathode is cut into a disk (10mm in diameter). Fourth, use lithium plate (anode) to assemble 2032 coin battery in glove box. Finally, the electrochemical performance of the assembled battery was tested for 12 hours.

3. RESULTS AND DISCUSSION

As shown in figure 1, all samples are consistent with the diffraction peak position of standard LiFePO4, which indicates that LiFePO4 has been successfully obtained [16, 17]. No excess impurity peak was observed in the prepared composite, indicating that LiFePO4 [18] is a pure olivine structure. In addition, all samples showed no characteristic peaks of carbon, which can be attributed to the excessive amount of carbon [19, 20]. The existence of sharp and well-defined Bragg peaks confirms the presence of phase pure and crystalline products.$LiFePO_4$/C composites exhibited standard orthorhombic olivine type $LiFePO_4$ structure (JCPDS 83-2092, a=10.33 Å, b= 5.98 Å, c= 4.69 Å). The diffraction peaks of carbon coated samples were enhanced compared with pure samples.

$LiFePO_4$/C with different carbon content was synthesized, and its peak area and half peak width were analyzed with Jade software as shown in the following table.

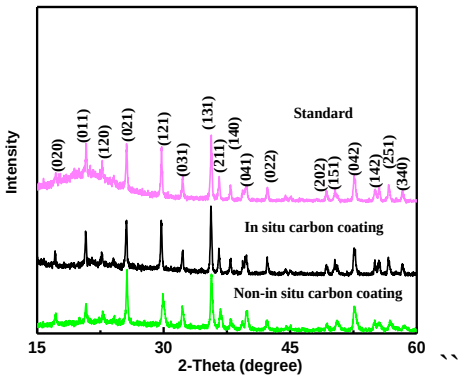

Figure 1. The XRD diagram of $LiFePO_4$/C synthesized in different carbon cladding methods

Table 1. Jade analysis table of LiFePO4/C synthesized in different carbon coating methods

Sample	2-Theta	Height	Area	FWHM
Standard	29.762	691	6518	0.160
In situ carbon coating	35.602	352	3956	0.191
Non-in-situ carbon coating	35.640	338	3878	0.195

Combined with table 1 analysis, In general, when the grain size reaches the nanometer level, Its XRD diffraction pattern will appear obvious broadening phenomenon compared with the ordinary matter. The size of grain size can be determined by Scherer formula [21]:

$$D = \frac{K\gamma}{B\cos\theta} \quad (1)$$

When the diffraction peak widens, the corresponding half-height-width of the diffraction peak increases, but delta and theta remain the same, the grain size D decreases.According to schellrrer formula,FWHM analysis of in-situ and non-in-situ carbon cladding was performed.The half-peak width (0.195) of non-in-situ carbon coating is larger than that of in-situ carbon coating (0.191). So the particle size of in-situ carbon coating is larger than that of non-in-situ carbon coating. This shows that at high temperature, the carbon source forms a carbonized film on the surface of the particle and covers the surface of $LiFePO_4$, inhibiting the growth of $LiFePO_4$ grains, increasing the carbon source content and decreasing the grains. This result is consistent with the Jade analysis.

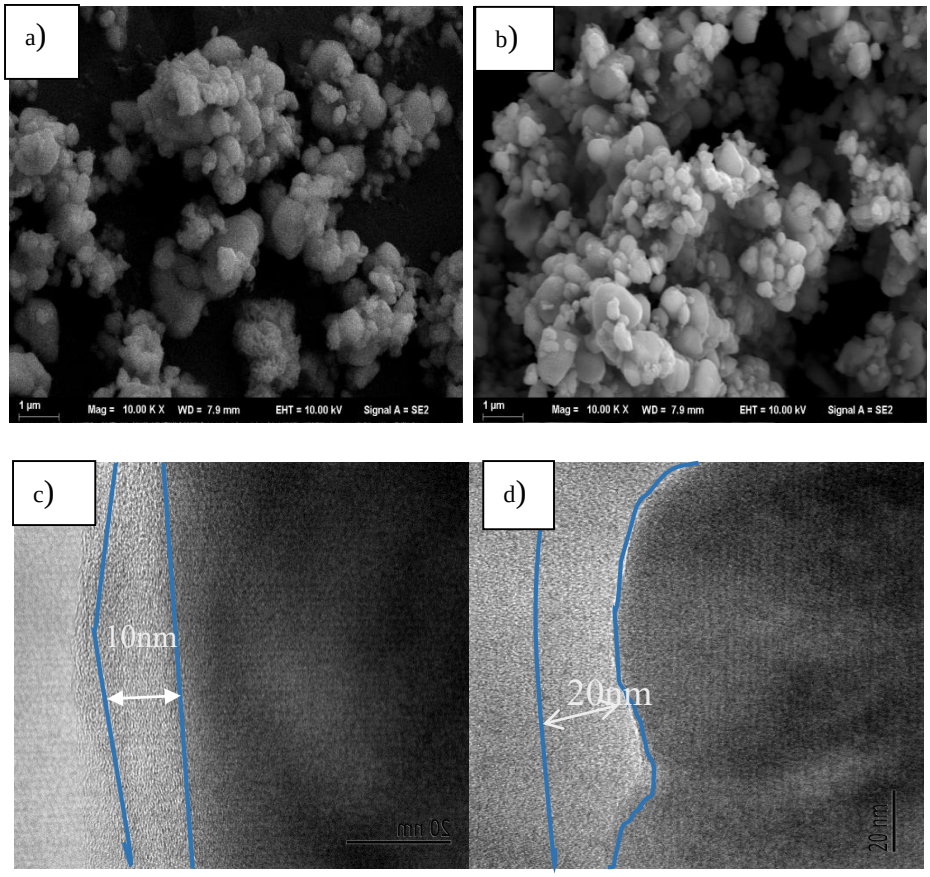

Figure 2. SEM and TEM charts of $LiFePO_4$/C synthesized by different proportions of carbon sources a)SEM images of in situ carbon coating; b)SEM images of non-in-situ carbon coating; c)TEM images of in situ carbon coating; d)TEM images of non-in-situ carbon coating

From the SEM micrographs, it is evident that the primary grains of in-situ carbon coating are nanometer in size and have good dispersibility as shown in Fig. 2a. As can be seen from Fig. 2b, The sample was nearly spherical with primary grain size of 600nm-800nm.Its boundary is obvious, covered with carbon layer, but there is certain agglomeration phenomenon. According to the TEM images in Fig. 2c and 2d, In situ carbon coating, the thickness of carbon layer is about 10 nm, while that of non-in-situ carbon coating is about 20 nm. The different ways of carbon coating are reflected in the different thickness of carbon layer in morphology [22]. The carbon layer can protect the morphology of samples from collapse at high temperature to some extent, and improve the conductivity of ions. On the surface of $LiFePO_4$ NPs, amorphous carbon is formed due to pyrolysis of glucose, so a good connection is formed between C and $LiFePO_4$ NPs. The in-situ carbon coating provides a high-speed electron transfer path and lithium ion migration rate, while the liquid electrolyte is more easily penetrated into the in-situ carbon-coated lithium iron phosphate material due to interconnected channels, which greatly improves The rate performance of the anode material. [23].

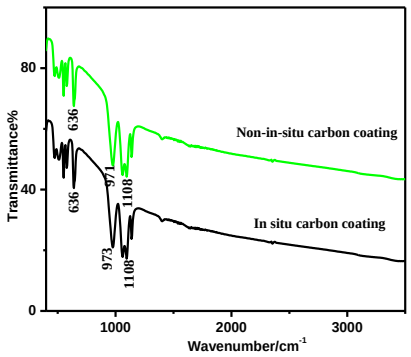

Figure 3. Infrared spectra of $LiFePO_4$/C synthesized in different proportions of carbon sources

The analysis is shown in figure 3, The infrared spectra of $LiFePO_4$/C synthesized by different carbon coating methods are basically consistent. There are three distinct characteristic absorption peaks, respectively located at 636 cm^{-1},973cm^{-1},1108cm^{-1}. The absorption peak at 636 cm^{-1} is the characteristic absorption peak of ferrous ions in $LiFePO_4$, which belongs to the symmetric stretching vibration absorption peak (V1). The characteristic absorption peak at 1063cm^{-1} is the characteristic absorption peak of PO_4^{3-} in $LiFePO_4$, which belongs to the anti-symmetric telescopic vibration absorption peak (V1) [24]. Because the polarity band of infrared detection is strong, the non-polarity band is assisted by Raman spectrum.

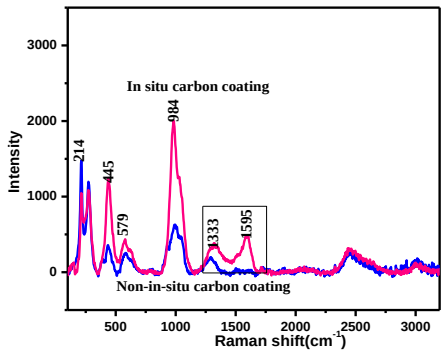

Figure 4. Raman spectra of $LiFePO_4$/C synthesized in different proportions of carbon sources

Raman spectrum, as a supplementary means of infrared characterization, can be obtained from the Raman spectrum analysis in Fig.4. At 1333cm^{-1} and 1595cm^{-1} respectively, these are characteristic Raman spectra of amorphous carbon in $LiFePO_4$/C material. Although the diffraction peak of carbon is not shown in the X-ray diffraction test, the characteristic peak of Raman spectrum is consistent with the carbon added in the synthesis process. The peak at the position next to 1333cm^{-1} and 1333cm^{-1} is the stretching vibration peak in PO_4^{3-} of $LiFePO_4$. Moreover, the carbon peak of samples prepared by non-in-situ carbon coating at 1595cm^{-1} was not obvious. The peak of 1333cm^{-1} is called peak D in Raman, and peak D represents the lattice defect of C atom. The peak at 1595cm^{-1} is called peak G [25], and peak G represents the in-plane stretching vibration of SP^2 hybrid of C atom. The larger proportion of G peak

indicates its good conductivity. In-situ carbon coating and non-in-situ carbon coating can obviously improve the graphitization degree in the material, which benefits the enhancement of conductivity.

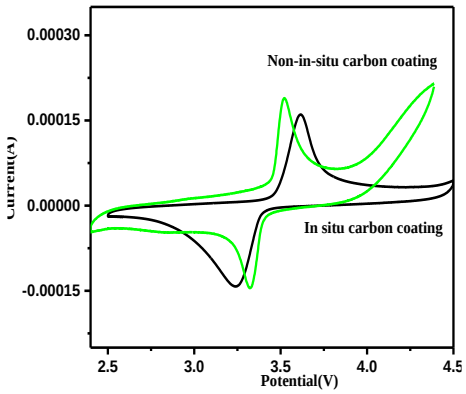

Figure 5. The cyclic voltammetry of $LiFePO_4/C$ with different proportions of carbon sources

It can be seen from the cyclic voltammetry curve analysis in Fig. 5, When using in situ carbon coated, cyclic voltammetric curves of oxidation and reduction peaks difference is small, meaning that its better reversibility, peak current and peak voltage value numerical difference is small, and the use of in-situ carbon coated, except a REDOX peak appeared in the oxidation peak position also increase a current, this is a unique polarization peak appeared. And the peak area decreases and the reversibility becomes worse. This is because the thickness of the carbon layer increases, which makes it difficult for lithium ions to be embedded and extruded, and the excess carbon intensifies the agglomeration of samples, resulting in a decline in their reversibility. The small difference between the redox peak current and voltage value of the CV curve with carbon coating means that it has good reversibility. From the point of view of peak area, when in-situ coating is used, its peak area is larger, and its specific capacity can be roughly calculated by using peak area. In general, the specific capacity of the CV curve with larger peak area will be larger.

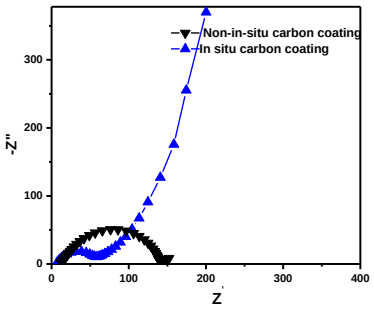

Figure 6. The impedance with different carbon cladding of carbon-coated $LiFePO_4/C$

According to the analysis in figure 6, the impedance of the samples synthesized by different carbon cladding methods is composed of a semicircle in the high-frequency region and a straight line in the low-frequency region. The current research shows that SEI membrane has a major impact on the

negative electrode and a small impact on the positive electrode, so it is not discussed in depth here. The other semicircular Rct is charge transfer resistance (electrochemical reaction resistance), and the Warburg impedance of the linear part is related to the diffusion of lithium ions in the active material. When non-in-situ carbon coating is adopted, its semicircle diameter is larger than that of in-situ carbon coating, indicating that the in-situ carbon coating charge transfer resistance is small, which leads to its high conductivity. The reason is that from Raman spectra and theoretical values,In-situ carbon coating has a relatively high conductivity. The difference here may be due to the deviation caused by the uneven thickness of carbon coating.

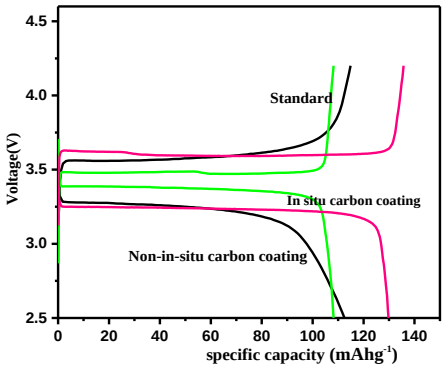

Figure 7. First Charge-Discharge Curve of $LiFePO_4$/C coated with carbon

As shown in figure 7, each sample has a complete charge-discharge platform, which indicates that the sample has good charge-discharge performance [26]. When $LiFePO_4$/C was prepared with in situ and non-in-situ carbon coating, its charge-discharge capacity was 125 $mAh \cdot g^{-1}$ and 112 $mAh \cdot g^{-1}$ respectively. However, the charge-discharge capacity of the anode material without carbon coating is 107 $mAh \cdot g^{-1}$, indicating that carbon coating has a great influence on its performance.

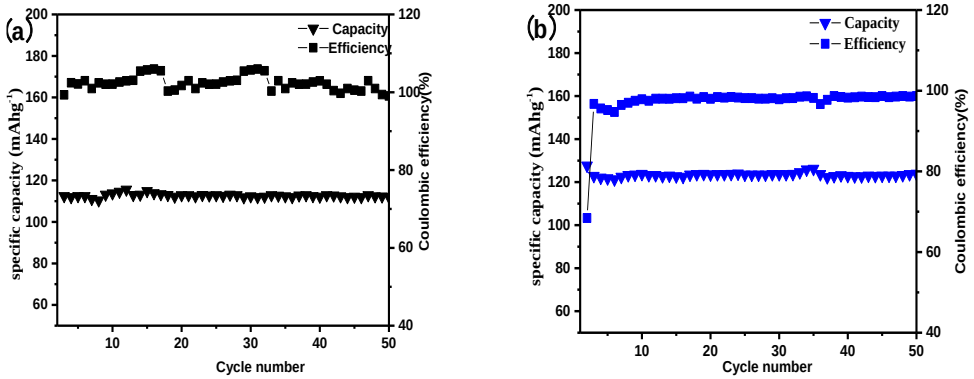

Figure 8. $LiFePO_4$/C Cycle Curves with different carbon cladding a)In situ carbon coating, b) Non-in-situ carbon coating

The charging and discharging platforms are all relatively long, which indicates that their charging and discharging voltage is stable. But at the same time, it can be concluded that the voltage of the voltage platform with non-in-situ carbon coating is relatively large, resulting in a large voltage difference [27],

which may be caused by the internal resistance of the battery. This is due to the decrease of resistance and polarization in the battery, which leads to the migration and diffusion of lithium ion in the conductive structure [28,29].

According to the analysis in figure 8, after the in-situ coating sample circulates for 50 times, the capacity attenuation is relatively small and the discharge capacity fluctuates slightly, but its coulombic efficiency fluctuates greatly, indicating that the reversibility of charge and discharge is weakened after 50 cycles, and the coating on the material surface is not uniform, resulting in inconsistent transmission paths of lithium ions and reduced reversibility. Although the cathode materials coated with carbon show good stability during charging and discharging, the in-situ carbon coating shows the best charge-discharge specific capacity and excellent electrochemical performance [30]. However, the specific capacity of $LiFePO_4$/C without in-situ carbon coating decreases significantly after 50 cycles, and its coulombic efficiency fluctuates greatly. This phenomenon is mainly affected by the thickness of the coating layer, indicating that the thinner the thickness of the carbon coating, the better of the performance. And when the carbon coating thickens, its performance is relatively poor. The in-situ carbon coating reduces the internal resistance of the cathode material, so the cycle performance is significantly improved [31,32]. The constructed conductive network can promote electron transport and lithium ion migration, and can stabilize the internal structure of the material, thus forming good cycle stability [33-35].

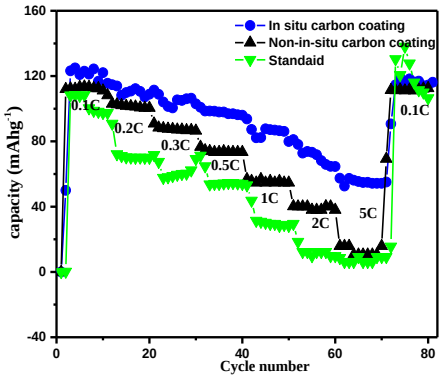

Figure 9. Discharge charts of $LiFePO_4$/C coated with carbon at different rates

According to the analysis of figure 9, $LiFePO_4$/C prepared by different carbon coating methods have different multiplier properties.With the in situ carbon coated, at high magnification, the specific capacity decline faster, such carbon source has no advantage in large current charge and discharge, and made of in-situ carbon coated samples under large discharge in situ carbon coating. In general, the specific capacity and multiple discharge performance of uncoated carbon and non-in-situ carbon coating are worse than that of in-situ carbon coating. The main reasons are as follows: the in-situ carbon coating can achieve molecular level mixing, which is more uniform, and can use its structural advantages as a template, which has a certain guiding effect on sample morphology.

4. CONCLUSIONS

For $LiFePO_4$/C synthesized by carbon coating, no matter it is non-in-situ coating or in-situ coating, it plays an important role in improving the electrochemical performance of $LiFePO_4$. Through the above comparison, the conclusions are as follows: When ascorbic acid was used as the carbon source, and the sample coating layers formed by in-situ carbon coating and non-in-situ carbon coating were 10nm and 20nm respectively. Through the electrochemical measurements, In situ carbon coated and non-in-situ carbon coated lithium iron phosphate, the specific capacity of charge and discharge for the first time reached 125 $mAh \cdot g^{-1}$ and 112 $mAh \cdot g^{-1}$ respectively at the rate of 0.1C. Compared with two different coating forms, the effect of in-situ carbon coating is better than that of non-in-situ carbon coating. The uniformity of non-in-situ carbon coating is not very good, and the over-thick coating makes it difficult to insert and remove lithium ions.

References

1. M. Zackrisson, L. Avellán, J. Orlenius, *J. Clean. Prod*., 18 (2010) 1519-1529.
2. B. Kang, G. Ceder, *Nature*, 458 (2009) 190-193.
3. Y. Shi, X. Y. Zhou, J. Zhang, A. M. Bruck, A. C. Bond, A. C. Marschilok, K. J. Takeuchi, E. S. Takeuchi, G. H. Yu, *Nano Lett.*, 17 (2017) 1906-1914.
4. K. Naoi, K. Kisu, E. Iwama, S. Nakashima, Y. Sakai, Y. Orikasa, P. Leone,N. Dupré, T. Brousse, P. Rozier, W. Naoi, P. Simon, *Energy Environ. Sci.*, 6 (2016) 2143-2151.
5. P. Xiong, Y. Choongho, *Nanoscale*, 4(21) (2012) 6743-7.
6. Chen, L. Zhu, D. Zhang, Y. Wei, Z. Zhang, S. Qiu, F. Pan, *Nano Energy*, 39 (2017) 346-354.
7. C. H. Tsao, C. H. Hsu, P. L. Kuo, *Electrochim. Acta*, 196 (2016) 41-47.
8. L. He, W. Zha, D. Chen, *J. Alloys Compd*., 727 (2017) 948-955.
9. C. Zheng, X.F. Zhou, H.L. Cao, G.H. Wang, Z.P. Liu, *J. Power Sources*, 258 (2014) 290-296.
10. S. Yang, M. Hu, L. Xi, R. Ma, Y. Dong, and C. Y. Chung, *ACS Appl. Mater. Interfaces*, 5 (2013) 8961-8967.
11. S. Lou, X. Cheng, Y. Zhao, A. Lushington, J. Gao, Q. Lia, P. Zuo, B. Wang, Y. Gao, Y. Ma, C. Du, G. Yin, X. Sun, *Nano Energy*, 34 (2017) 15-25.
12. Z. Ma, Y. Fan, G. Shao, G. Wang, J. Song, T. Liu, *ACS Appl. Mater. Interfaces*, 7 (2015) 2937-2943.
13. N. HaiFang, L. JinKun, F. Li-Zhen, *Nanoscale*, 5(5) (2013) 2164-2168.
14. R. Mei, Y. Yang, X. Song, Z. An, K. Yan, J. Zhang, *Electrochim. Acta*, 218 (2016) 325-334.
15. X. Wang, Z. Feng, J. Huang, W. Deng, X. Li, H. Zhang, Z. Wen, *Carbon*, 127 (2018) 149-157.
16. X. Lei, H. Zhang, Y. Chen, W. Wang, Y. Ye, C. Zheng, P. Deng, Z. Shi, *J. Alloys Compd*., 626 (2015) 280-286.
17. E. Meng, M. Zhang, Y. Hu, F. Gong, L. Zhang, F. Li, *Electrochimica Acta*, 265 (2018) 160-165.
18. D. Jang, K. Palanisamy, J. Yoon, Y. Kim, W.S. Yoon, *J. Power Sources*, 244 (2013) 581-585.
19. J.K. Kim, J.W. Choi, G.S. Chauhan, J.H. Ahna, G.C. Hwang, J.B. Choi, H.J. Ahn, *Electrochim. Acta*, 53 (2008) 8258-8264.
20. R. Malik, D. Burch, M. Bazant, G. Ceder, *Nano Lett*., 10 (10) (2010) 4123-4127.
21. P.M. Pratheeksha, E.H. Mohan, B.V. Sarada, M. Ramakrishna, K. Hembram, P.V. Srinivas, P.J. Daniel, T.N. Rao, S. Anandan, *Phys. Chem. Chem. Phys*., 19 (2016) 175-188.
22. H. Guo, H. Ping, J. Hu, X. Song, J. Zheng, F. Pan, *J. Mater. Chem. A*, 5 (2017) 14294-14300.

23. X. Lei, H. Zhang, Y. Chen, W. Wang, Y. Ye, C. Zheng, P. Deng, Z. Shi, *J. Alloys Compd*., 626 (2015) 280-286.
24. J. Tu, K. Wu, H. Tang, H. Zhou, S. Jiao, *J. Mater. Chem*. A 32 (2017) 17021-17028.
25. A.B. Kanagaraj, P. Chaturvedi, T.S. Alkindi, R.A. Susantyoko, B.H. An, S.P. Patole, K. Shanmugam, S. AlMheiri, S. AlDahmani, H. AlFadaq, D.S. Choi, *Mater. Lett.*, 230 (2018) 57-60.
26. H. Tian, X. Zhao, J. Zhang, M. Li, H. Lu, *ACS Appl. Energy Mater*., 1 (2018) 3497-3504.
27. H. Zhong, A. He, J. Lu, M. Sun, J. He, L. Zhang, *J. Power Sources*, 336 (2016) 107-114.
28. G. Longoni, J.K. Panda, L. Gagliani, R. Brescia, L. Manna, F. Bonaccorso, V. Pellegrini, *Nano Energy*, 51 (2018) 656-667.
29. T. Tsuda, N. Ando, K. Matsubara, T. Tanabe, K. Itagaki, N. Soma, S. Nakamura, N. Hayashi, T. Gunji, T. Ohsaka, F. Matsumoto, *Electrochimica Acta*, 291 (2018) 267-277.
30. J. J. Bao, B. K. Zou, Q. Cheng, Y. P. Huang, F. Wu, G. W. Xu, C. H. Chen, *J. Membrane Science*, 541 (2017) 633-640.
31. Y. Liu, J. Wang, J. Liu, M.N. Banis, B. Xiao, A. Lushington, W. Xiao, R. Li, T.-K. Sham, G. Liang, X. Sun, *Nano Energy*, 45 (2018) 52-60.
32. L. Yang, X. Li, S. He, G. Du, X. Yu, J. Liu, Q. Gao, R. Hua, M. Zhu, *J. Mater. Chem*. A 4 (2016) 10842-10849.
33. Z. Cao, G. Zhu, R. Zhang, S. Chen, M. Sang, J. Jia, M. Yang, X. Li, S. Yang, *Chem. Eng. J.*, 351 (2018) 382-390.
34. Y. Zou, G. Chang, S. Chen, T. Liu, Y. Xia, C. Chen, D. Yang, *Chem. Eng. J.*, 351 (2018) 340-347.
35. D. Rueda-Garcia, Z. Cabán-Huertas, S. Sánchez-Ribot, C. Marchante, R. Benages, D.P. Dubal, O. Ayyad, P. Gómez-Romero, *Electrochimica Acta*, 281 (2018) 594-600.